Progress in Flight Physics **9** (2017) 25-42
DOI: 10.1051/eucass/201709025

STARTING OF GENERIC INLET WITH BLUNTED WEDGES

V. Borovoy, V. Mosharov, V. Radchenko, A. Skuratov, and I. Struminskaya

Central Aerohydrodynamic Institute (TsAGI)
1 Zhukovsky Str., Zhukovsky, Moscow Region 140180, Russia

Bluntness effect of gas-compressing wedges on starting and flow structure in an air inlet was investigated experimentally. The inlet was of internal compression type with flat walls and rectangular cross section. The experiments were carried out in the wind tunnel UT-1M at Mach numbers $M = 5$ and 8 and Reynolds numbers $Re_{\infty L}$ from $2.8 \cdot 10^6$ to $23 \cdot 10^6$. The flow characteristics were measured by panoramic optical methods. Data demonstrating influence of wedge bluntness radius on the inlet starting were obtained at different Mach and Reynolds numbers as well as at different contraction ratios. Ambiguity of the flow regime in the inlet under certain conditions was found.

1 INTRODUCTION

Starting of supersonic inlet is an interesting problem both from theoretical and practical points of view and attracted many researches (see, for example, [1–16]). The problem arises when the inlet is shaped as a converging channel. In order to provide the inlet starting, one should limit the channel constriction that results in limiting of air compression.

It is known that leading edges of a hypersonic inlet should be blunt to exclude the surface overheating. Moreover, the sharp leading edges will be blunted during a hypersonic flight due to ablation. In [4], it is shown that blunting of leading edges can result in significant decrease of pressure recovery and mass flow rate as well as in unstart of the inlet. However, most other studies deal with sharp leading edges. Maybe, there was supposed that the leading edge bluntness plays a secondary role in the gas flow. But in reality, as the present investigation shows, even small blunting of the leading edges at high contraction ratio can influence the inlet starting similar to the significant increase of Mach number or decrease of Reynolds number.

In this work, a schematized inlet of internal compression type with flat walls and rectangular cross section was studied. Such inlets are not used practically, but the observed phenomena can meet with real flow configurations.

The present paper is the completion of studies started in [15] and continued in [16]. The subject of the study in [15] was a pair of wedges located on sharp or blunt plate. In [16], the pair of wedges was replaced by the inlet and the influence of plate- and cowl-bluntness on the flow was investigated. In the present paper, the same model as in [16] was used, but the study is focused on the wedge-bluntness effect on the inlet starting.

2 TEST MODEL CONFIGURATION AND FLOW CONDITIONS

Figure 1 presents the experimental model. On the flat plate *1*, the wedges *2* with cowl *3* are located. The wedges have changeable leading edges *4* for variation of the bluntness radius in the range from 0 to 4 mm. The cowl is transparent behind the leading edge to provide the visibility of the flow inside the inlet. In some tests, the wedge manufactured of a transparent material was used. The shape of the model studied can be characterized by the following nondimensional values affecting the flow in the inlet: the relative distance of the inlet from the plate leading edge $X_0/W_0 = 1.29$ and the relative inlet height $H/W_0 = 0.8$. The channel contraction ratio $\eta = W_0/W_t$ was varied by replacement the wedges: when the wedge thickness was 37.5 mm, the throat width was 25 mm and

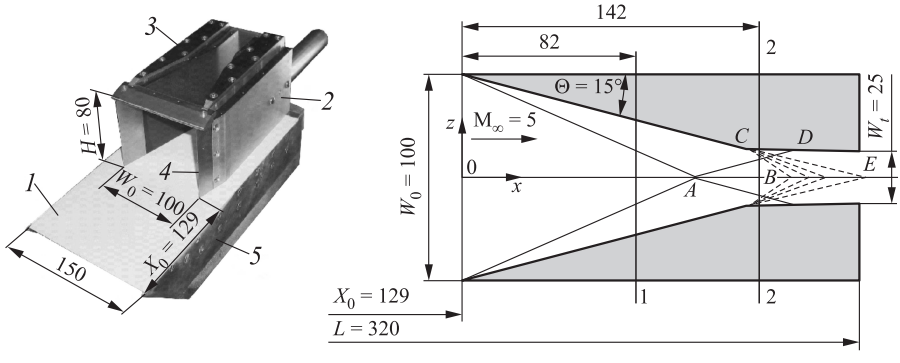

(*a*) (*b*)

Figure 1 Photograph of the model (*a*) and cross section of the wedges (*b*): *1* — plate; *2* — wedges; *3* — cowl; and *4* — changeable leading edges of the wedges. Dimensions are in millimeters

Table 1 Flow characteristics

Mach number	Reynolds number $\mathrm{Re}_{\infty L}$	Total pressure P_t, bar	Total temperature T_t, K
5	$8.5 \cdot 10^6$	23.3	520
	$13 \cdot 10^6$	33.6	520
	$23 \cdot 10^6$	62.9	530
8	$2.8 \cdot 10^6$	43.0	750
	$5.6 \cdot 10^6$	89.0	770

$\eta = 4$. Correspondingly, when the wedge thickness was 33.3 mm, the throat width was 33.3 mm and $\eta = 3$.

Figure 1*b* illustrates the shock waves and rarefaction waves in the two-dimensional (2D) flow of nonviscous gas at M = 5. Behind the wedge shocks, the pressure is 4.8 times higher in respect with the undisturbed flow. The shock reflected from the symmetry line increases the pressure 3.4 times additionally. Thus, the pressure inside the rhombus located between the points A and B is 16.4 times higher than that in the undisturbed flow. Between the points C and D, the pressure falls almost to the undisturbed level ($P/P_\infty = 1.08$).

The tests were carried out in the TsAGI wind tunnel UT-1M. It worked in the Ludwieg-type mode. The steady flow duration was 40 ms. The averaged characteristics of undisturbed flow are presented in Table 1.

Scatter of total pressure values in different runs was ±6% of the mean pressure at $P_t = 62.9$ bar and ±10% at $P_t = 33.6$ bar. The total temperature scatter was ±2%. The surface temperature was approximately 293 K; so, the temperature factor T_w/T_0 at $\mathrm{M}_\infty = 5$ was 0.56 and at M = 8, it was 0.39.

3 EXPERIMENTAL METHODS

Investigations of heat transfer and pressure distribution were performed by the thin luminescent paints sensitive to the temperature or to the pressure, correspondingly [17]. The methods use the temperature quenching of luminescence of organic dye. At heat-transfer investigation, the measured increase of temperature during the determined time interval is used to calculate the heat flux from gas to the surface in each point. The surface flow is visualized by the method recently developed at TsAGI [18]. It is based on measurements of small movements of oil marked by contrast fluorescent particles. In addition, the method presents visulization of shear stress distribution.

The above described methods are applied in the present work similar to [16] for investigation of external and internal flow as well. To do that, some parts

of the cowl and one wedge were made of a material transparent to the exciting ultraviolet (UV) light and to the luminescent visible light. The transparent parts were used in two ways: (*i*) to measure the heat flux to the transparent surface; and (*ii*) to measure the heat flux to the opposite nontransparent surface. Thermal characteristics of appropriate material were used at solving the equation of heat diffusion. The data presented below demonstrate a satisfactory agreement between the experimental results and calculated heat flux values on the cowl and on the plate under the cowl.

According to the estimations, the total related measurement error lies in the range from 10% to 30% depending on the absolute value of heat flux and pressure.

4 STARTING OF A CONVERGENT CHANNEL

The channel can be referred as started if the channel "swallows" the supersonic jet coming to the front area of the channel W_0 (Fig. 2, left). In contrast, if some part of the coming jet "splash out" and does not get inside the channel, the channel is referred as unstarted (Fig. 2, right).

Considering the staring process in the one-dimensional (1D) approach at constant characteristics of undisturbed supersonic flow, one can determine three ranges of contraction ratio $\eta = W_0/W_t$ (see Fig. 2, W_t is the throat width).

(1) if $\eta < \eta_1$, the channel is always started and a supersonic flow exists inside the channel. Autostarting is provided, and no starting device is necessary;

(2) if $\eta_1 < \eta < \eta_2$, two flow regimes are possible: with supersonic speeds inside the channel (started channel) or with subsonic speeds inside the channel (nonstarted or blocked channel). In the second case, the bow shock wave forms in front of the channel and some part of the coming jet, corresponding

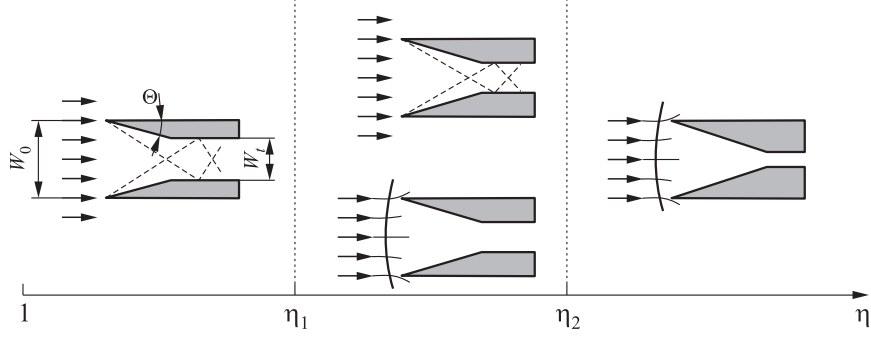

Figure 2 Ranges of channel contraction ratio

to the entrance area W_0, flow outside. The implementation of the regime depends on the prehistory of the flow. At nonstart, the total pressure losses are higher than at start; and

(3) if $\eta > \eta_2$, starting of the channel is impossible and the flow with detached bow wave realizes.

The value of η_1 can be determined from the mass flow rate equation

$$\rho_\infty U_\infty W_0 = \rho_* U_* W_t\,; \qquad (1)$$
$$\eta_1 = \frac{\rho_* U_*}{\rho_\infty U_\infty}\,.$$

Here, ρ_∞ and U_∞ are the gas density and velocity in the undisturbed flow; and ρ_* and U_* are similar values in the channel throat. It assumed that normal shock forms ahead the channel entrance. Behind the normal shock, between the channel entrance and throat, gas accelerates isentropic to the sound speed U_* and its density decreases to the corresponding value ρ_*. Equation (1) implies the Kantrovitz' relation [1]:

$$\frac{1}{\eta_1} = \left[\frac{\gamma-1}{\gamma+1} + \frac{2}{\gamma+1}\,\mathrm{M}_\infty^2\right]^{1/2} \left[\frac{2\gamma}{\gamma+1} - \frac{\gamma-1}{\gamma+1}\,\mathrm{M}_\infty^2\right]^{1/(\gamma-1)} \qquad (2)$$

where $\gamma = C_p/C_v$ is the ratio of specific heats at constant pressure and volume.

According to (2), the values of η_1 are small: at $\mathrm{M}_\infty = 5$, $\eta_1 = 1.54$; at $\mathrm{M}_\infty = 8$, $\eta_1 = 1.61$; and at $\mathrm{M}_\infty = \infty$, $\eta_1 = 1.67$ ($\gamma = 1.4$). Respectively, the gas compression rate is also small. Therefore, the application of inlets with bigger contraction ratio ($\eta > \eta_1$) is of practical interest.

At $\eta > \eta_1$, the maximal contraction ratio η_2, permitting the supersonic flow inside the channel, is also limited by the channel throat, and the value of η_2 can be also obtained from Eq. (1). But in this case, the gas density in the throat should be defined using the value ρ_∞ and taking into account the total-pressure losses in the channel due to the gas viscosity and presence of shock waves. In the special case of isentropic flow (similar to the contrary Laval nozzle), $\eta_2 = 25$ at $\mathrm{M}_\infty = 5$ and $\eta_2 = 190$ at $\mathrm{M}_\infty = 8$. But the total-pressure losses in the shock waves decrease significantly the η_2-values: for the 2D inviscid flow in the channel, shown in Fig. 1*b*, $\eta_2 = 14.7$ at $\mathrm{M}_\infty = 5$ and $\eta_2 = 51$ at $\mathrm{M}_\infty = 8$. Gas viscosity and blunting of leading edges diminish additionally the η_2-values, as will be shown below.

Influence of gas viscosity and leading-edges bluntness can be assessed approximately substituting the real throat width by an effective width $W_t - 2(\delta^* + \Delta^*)$ where δ^* and Δ^* are the thicknesses of boundary and high-entropy layers. Then, let us obtain for the effective channel contraction ratio:

$$\eta_{\text{ef}} = \frac{W_0}{W_t - 2(\delta^* + \Delta^*)}\,,$$

or

$$\eta_{\text{ef}} = \frac{\eta}{1 - 2(\delta^* + \Delta^*)/W_t}\,.$$

The effective coefficient of channel contraction η_{ef} does not consider the losses in the internal shocks. It also does not consider the three-dimensional (3D) effects of interference between the wedge shocks and the boundary layers generated on the plate and cowl surfaces. Therefore, the η_{ef}-value is not a stringent criterion of inlet blockage. It reflects only the trend approaches the blockage or away from it at variations of bluntness radius and Reynolds number. The presented below data show that the inlet under study approaches the blockage when η_{ef} closes to the value $\eta_{\text{ef}} = 4.5$ at $\text{M} = 5$ and to $\eta_{\text{ef}} = 4$ at $\text{M} = 8$.

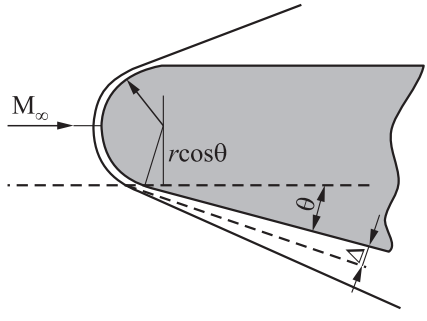

Figure 3 Formation of a high-entropy layer

The thickness of high-entropy layer can be estimated by assuming the following [19] (Fig. 3): the bow shock wave is equidistant to the leading edge surface; the thickness of the jet deflected download (on the declined surface of the wedge) is equal $r\cos\theta$; gas expands isentropic from the total pressure behind the normal shock P_{st} to the pressure on the inclined surface of the sharp wedge P_e; and the high-entropy layer is uniform. The equation of mass flow rate gives

$$\rho_\infty U_\infty r\cos\theta = \rho_\Delta U_\Delta \Delta\,,$$

or

$$\frac{\Delta}{r} = \frac{P_\infty}{P_e}\,\frac{T_\Delta}{T_\infty}\,\frac{U_\infty}{U_\Delta}\,\cos\theta\,. \tag{3}$$

Here, Δ is the thickness of high-entropy layer; and ρ_Δ, T_Δ, and U_Δ are the gas density, temperature, and speed in the high-entropy layer at big distance from the wedge leading edge. The last values can be estimated in dependence on the ratio P_e/P_{st}. The following relation can be obtained for the displacement thickness of high-entropy layer Δ^* (subscript e refers to the nonviscid flow on the sharp wedge):

$$\frac{\Delta^*}{\Delta} = 1 - \frac{T_e}{T_\Delta}\,\frac{U_\Delta}{U_e}\,.$$

The relation (3) shows that high-entropy layer gets thinner when wedge angle θ increases due to the increase of pressure P_e and thinning the jet deflected on the inclined surface of the wedge. For the angle $\theta = 15°$, the following estimates have been obtained: $\Delta^*/r = 0.46$ at M = 5 and $\Delta^*/r = 0.62$ at M = 8.

Starting of the inlet with contraction ratio $\eta_1 < \eta < \eta_2$ in a wind tunnel depends on the character of flow start in the wind tunnel [7, 8]. In the impulse wind tunnel, usually, the "wave" start takes place. It means that the nozzle and the test chamber are vacuumed before the start. Then, the shock wave passes through the nozzle of the wind tunnel and through the channel of the inlet. At that, the supersonic flow realizes usually in the inlet. But in the present study, it is revealed that in the inlets with contraction ratios $\eta_1 < \eta < \eta_2$ at some flow characteristics, both subsonic or supersonic flow regime can realize (see below).

In contrast, in long-duration wind tunnel, the flow start is usually slow. At that, in the inlet with contraction ratio $\eta_1 < \eta < \eta_2$, the subsonic flow with bow shock wave is always set.

5 FLOW PATTERNS

The presented below experimental data demonstrate that one of three flow patterns shown in Fig. 4 can realize in the inlets under investigation.

Regular flow with internal shocks forms at low influence of gas viscosity and small bluntness of the leading edges (Fig. 4*a*). The shocks generate narrow local separation zones, in which gas flows spirally in normal direction. The flow near each wedge is the same as near the single wedge up to the point of intersection between the boundaries of wedge-influence regions. Behind this point, a more complicated flow structure forms. It is investigated in detail in [20].

Symmetrical global separation zone (Fig. 4*b*) forms at blockage of a channel with moderate contraction ratio. If the inlet is located near the plate leading edge, the detached bow wave would be formed in front of the inlet. Due to the big distance from the plate leading edge to the inlet, the interference between the bow shock wave and plate boundary layer leads to formation of global separation zone and separation shock (see Fig. 4*b*). Location of the separation line depends on the related inlet height H/X_0 (see Fig. 1). At large values H/X_0, the separation line is located near the plate leading edge. The separated boundary layer reattaches inside the inlet, near the wedges and the throat.

Formation of nonsymmetrical global separation zone with reverse flow is possible in the inlet with big contraction ratio. In this case, the boundary of the separation zone ahead the inlet is conical as shown in Fig. 4*c*. But at some tests, symmetrical separation zone shown in Fig. 4*b* was observed at large contraction ratio, as well.

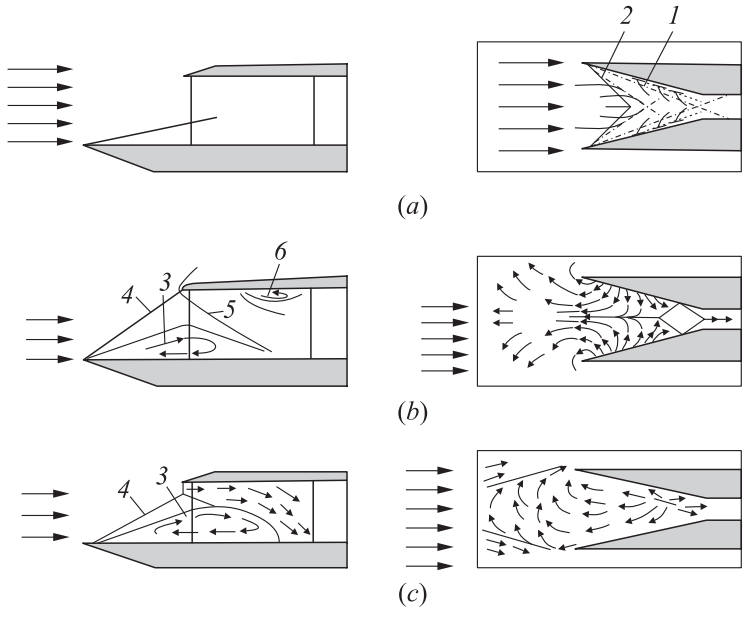

Figure 4 Flow patterns: (*a*) regular flow; (*b*) symmetrical flow in the blocked channel; (*c*) nonsymmetrical flow in the blocked channel; *1* — wedge shock; *2* — local separation shock; *3* — global separation zone; *4* — global separation shock; *5* — bow wave generated by the cowl; and *6* — separation zone on the cowl

6 EXPERIMENTAL DATA. FLOW STRUCTURE AND HEAT TRANSFER

Flow structure and heat transfer were studied mainly at Mach number M = 5. Figure 5 demonstrates impact of wedge-leading-edge bluntness on heat transfer over the plate and cowl surfaces.

At the cowl absence (Fig. 5*a*), regular flow with local separation zones, generated by the wedges, forms even at large wedge bluntness radius $r = 2$ mm and at high contraction ratio $\eta = 4$. It happens because some part of the gas, compressed by the shocks, flow out along the wedges.

At the cowl presence (Fig. 5*b* and 5*c*), the regular flow persists when the wedges are sharp or blunted weakly. But significant blunting, for example, by the radius $r = 2$ mm, results in high total-pressure losses and leads to the channel blockage and formation of global separation zone. The flow can be symmetric or nonsymmetric. At the test, demonstrated in Fig. 5*b* (right), the separation flow was nonsymmetric and the separation zone was conical in front of the channel. Near the top boundary of the separation zone, where the flow reattaches to

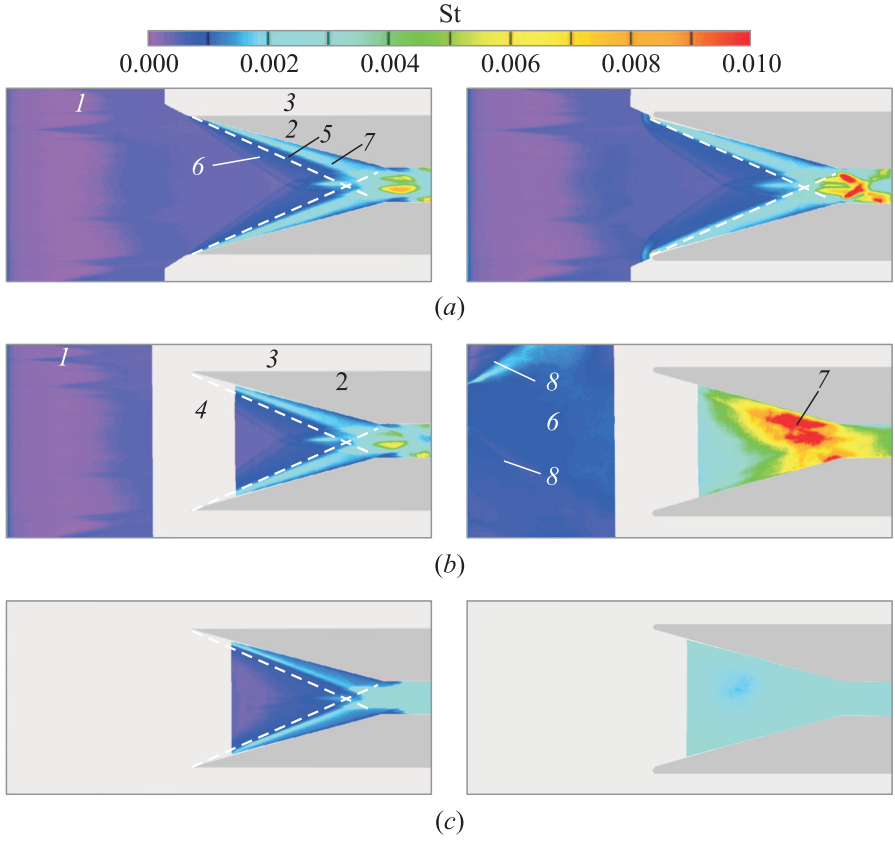

Figure 5 Distribution of Stanton number on the plate and inner surface of the cowl at M = 5, $\mathrm{Re}_{\infty L} = 23 \cdot 10^6$, and $\eta = 4$: (*a*) the plate at the cowl absence; (*b*) the plate at the cowl presence; (*c*) the cowl; *1* — the plate; *2* — the wedges; *3* — shadows of the wedges; *4* — nontransparent part of the cowl; *5* — shocks; *6* — separation zones; *7* — reattachment zones; and *8* — boundaries of the separation zone on the plate. Left column refers to $r = 0$ mm and right column to $r = 2$ mm

the plate, heat transfer was enhanced and near the opposite boundary, it was weakened. Similar nonsymmetry of heat transfer distribution was inside the channel.

Figure 6 gives additional information concerning the flow pattern inside the inlet at large wedge bluntness when nonsymmetrical separation zone forms. The picture presents stream lines and visualizes shear stress distribution as well. On the cowl, a converging line can be seen in front of the throat. The line is removed from the channel symmetry line. Near the cowl, only some part of flow

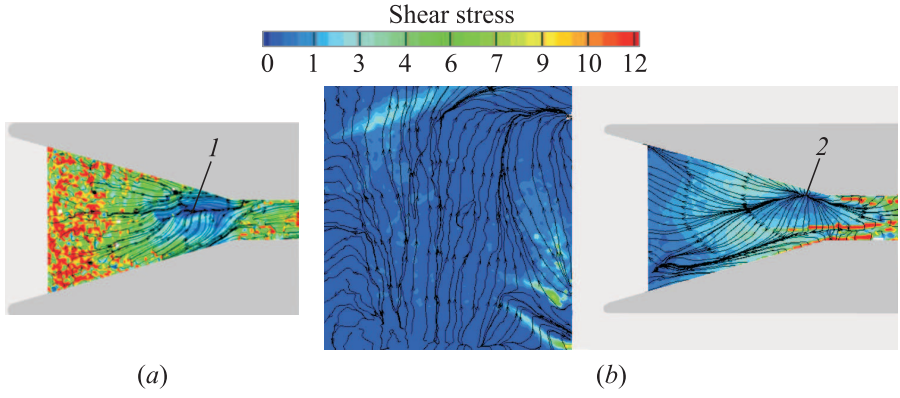

Figure 6 Surface stream lines and shear stress visualization in the inlet with blunted wedges ($r = 4$ mm) at M = 5, $\mathrm{Re}_{\infty L} = 23 \cdot 10^6$, and $\eta = 4$: (*a*) cowl; (*b*) plate; *1* — convergence line; and *2* — divergence line

penetrates into the throat and significant part of gas flows down to the plate. The convergence line is similar to the line of sinks. Line of sources is formed on the plate (see Fig. 6*b*), under the line of sinks. From the source line, gas flows to the plate leading edge and to the throat as well. The shear stress distribution corresponds to the flow pattern: on the cowl (see Fig. 6*a*), shear stress decreases with the distance from the leading edge due to the thickening of the boundary layer and reaches a minimum at the convergence line; and on the plate (see Fig. 6*b*), the shear stress at first increases with the distance from the source line due to the flow acceleration and then decreases with thickening of the boundary layer.

Distribution of pressure coefficient C_P is presented in Fig. 7 for the same conditions as St-number distribution. At the sharp wedges, the C_P-distribution is similar to the St-distribution: local increase of pressure occurs behind the separation zones generated by the wedges and in the intersection of the separation zones. Much higher pressure increase is visible behind the wedge shocks and behind the shocks intersection point. But at big bluntness of the wedges, the pressure distribution is symmetrical in contrast to the St-number distribution. At that, almost isobarick region forms on the plate in front of the inlet. The reasons of formation of symmetric or nonsymmetric separation zones are not established. Apparently, the separation flow is not stable and sensitive to small difference in the wedge angle relative the flow direction.

In the range from 0 to 1 mm, i. e., at regular flow in the inlet, the variation of bluntness radius influences weakly the St-number distribution. Figure 8 demonstrates St-number distribution along the symmetry line of the plate and the cowl at two values of wedge bluntness: $r = 0$ and 2 mm. At $r = 0$ mm, laminar–

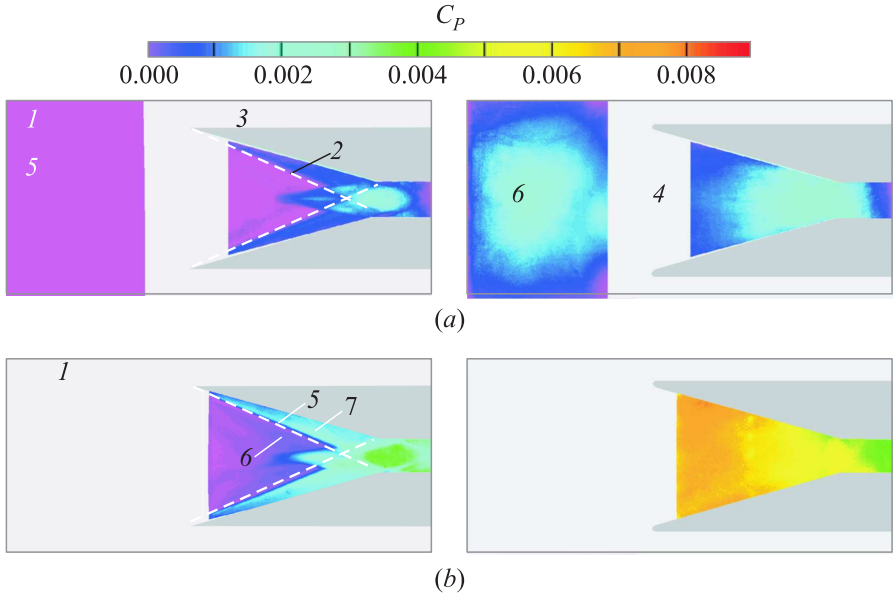

Figure 7 Distribution of pressure coefficient C_P in the inlet with cowl at M = 5, $\mathrm{Re}_{\infty L} = 23 \cdot 10^6$, and $\eta = 4$: (*a*) plate; and (*b*) cowl. The notations are the same as in Fig. 5. Left column refers to $r = 0$ mm and right column to $r = 2$ mm

turbulent transition occurs at the distance about 80 mm from the plate leading edge so that the wedge shocks interact with the turbulent boundary layer. On the cowl, the distance from the leading edge to the shocks intersection point is shorter, and the wedge shocks interact with the laminar boundary layer. But inside the separation zones, the transition occurs. This is testified by the comparison of maximum values of St-number on the cowl and on the plate: they are close to each other. Blunting the wedges with $r \geq 2$ mm leads to the blockage the inlet and to significant increase of St-number both on the plate and on the cowl. The maximal St-number on the cowl is much lower than on the plate (see Fig. 8) because the separation shock does not reach the cowl.

In the undisturbed region on the sharp plate (at $X < 190$ mm), the experimental data are close to the predictions for laminar and turbulent boundary layers (see Fig. 8*a*). This concerns the measurements ahead the inlet ($X < 129$ mm) and inside it ($165 < X < 190$ mm) as well and demonstrates acceptable accuracy of the heat-transfer measurements on the plate through the transparent cowl. Consistency of the measurements with calculations on the cowl itself ($X = 150$–176 mm, see Fig. 8*b*) is not so good. This can be connected both with measurements errors and the forward shock influence along the laminar flow.

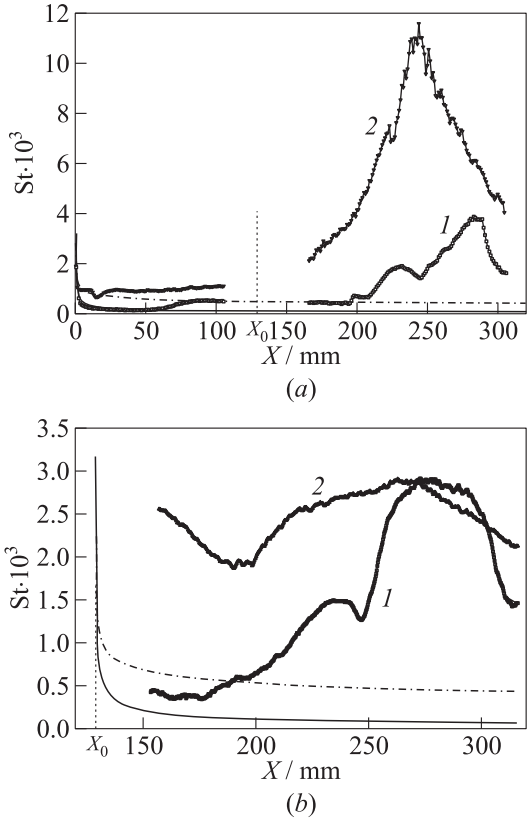

Figure 8 Stanton number distribution along the symmetry line of the plate (a) and of the cowl (b) at M = 5, $\mathrm{Re}_{\infty L} = 23 \cdot 10^6$, and $\eta = 4$: *1* — $r = 0$ mm and *2* — $r = 2$ mm

At regular flow, on the symmetry line of the plate and the cowl, two maxima are seen (see Fig. 8). The first one corresponds approximately to the intersection point of the separation shocks (here, St-number is 4 times bigger than in front of the interference region). The second maximum corresponds to the intersection point of the shocks generated by the wedges. At this point, St-number increases 10–15 times depending on the flow regime.

Figure 9 demonstrates heat transfer distribution on the inner surface of the sharp wedge at the presence of sharp cowl and slightly blunted plate. The panoramic investigation showed weakly variation of the heat transfer coefficient along the height of the wedge; therefore, the St-distribution is presented for the middle section ($Y = 40$ mm) only. Comparison of the experimental data with the prediction shows that at M = 5 and $\mathrm{Re}_{\infty L} = 23 \cdot 10^6$, the transi-

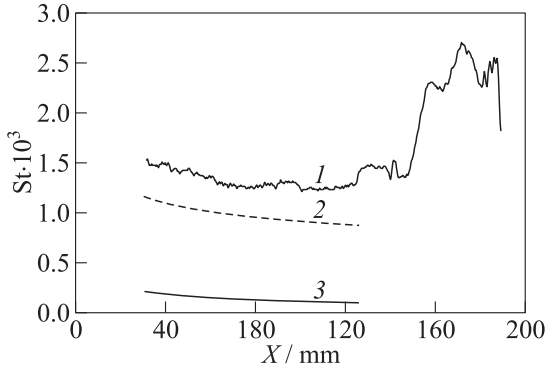

Figure 9 Stanton distribution along the symmetry line of the wedge at M = 5 and $\mathrm{Re}_{\infty L} = 23 \cdot 10^6$: *1* — experiment; *2* — prediction for the turbulent boundary layer; *3* — prediction for the laminar boundary layer; $X = 0$ corresponds to the wedge leading edge

tion occurs on the wedge surface near its leading edge. At the same conditions, as shown above, laminar flow is maintained on the cowl up to the region of interference between the wedge shocks. The difference is partly due to the pressure increase and, correspondingly, to the increase of the local Reynolds number (approximately 1.5 times). Maybe, more important was the influence of shock vibrations.

7 INFLUENCE OF WEDGE BLUNTNESS ON THE INLET BLOCKAGE

The St-number value on the plate at the point with coordinates $X = 235$ mm and $Z = 0$ (see Fig. 8*a*) is used as the indicator of inlet blockage. Near this point, the first pick of heat transfer coefficient forms. The St-number at this point varies slightly with wedge bluntness but only until the regular mode of flow maintains. When the inlet blockage happens, the St-number increases sharply. Figure 10 presents St-number at the characteristic point ($X = 235$ mm and $Z = 0$) in dependence on the related bluntness radius r/W_t at M = 5.

From Fig. 10, it follows that blockage of the inlet with $\eta = 4$ occurs at related wedge bluntness $r/W_t = 0.06$ ($r = 1.5$ mm), and the inlet with smaller contraction ratio $\eta = 3$ is started even at maximal value of related bluntness radius studied $r/W_t = 0.12$ ($r = 4$ mm) (in Fig. 10 and following figures, the started inlets are marked by open symbols and the unstarted ones by filled symbols). The boundary layer on the wedges near the throat is turbulent as can

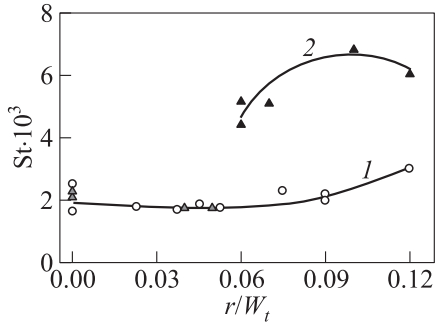

Figure 10 Influence of channel contraction ratio η on the inlet blockage at M = 5 and $\mathrm{Re}_{\infty L} = 22 \cdot 10^6$: *1* — $\eta = 3$ and $W_t = 33.3$ mm; *2* — $\eta = 4$ and $W_t = 25$ mm; open symbols correspond to the started inlet; and filled symbols correspond to the unstarted inlet

be concluded from Fig. 9. Thus, for the blockage conditions of the inlet with $\eta = 4$, the following estimation can be obtained: displacement thickness of the high-entropy layer generated by the wedge leading edges is $\Delta^* = 0.9$ mm at $r = 1.5$ mm, displacement thickness of turbulent boundary layer on the wedge surface near the throat is $\delta^* = 0.79$ mm (at that, the Reynolds number, calculated using the local flow characteristics and the length $S = 145$ mm, is $\mathrm{Re}_{e,S} = 16 \cdot 10^6$); the effective contraction ratio is $\eta_{ef} = 4.6$. For the inlet with $\eta = 3$, the maximal tested bluntness radius is $r_3 = 4$ mm, the corresponding displacement thicknesses are $\Delta^* = 2.4$ mm and $\delta^* = 0.72$ mm, and corresponding value of the effective contracting ratio is $\eta_{\mathrm{ef}} = 3.7$. This value is much lower than in the previous case that correlates with the fact that at $\eta = 3$, the channel is started. Assuming that the critical value of contraction ratio is the same in both cases ($\eta_{\mathrm{ef}} = 4.6$), the blockage of the channel with $\eta = 3$ should occur at wedge bluntness radius $r_3 = 8.5$ mm.

Reynolds number has a great influence on the inlet blockage (Fig. 11). As mentioned above, blunting the wedges up to $r = 4$ mm ($r/W_t = 0.12$ and $\eta_{\mathrm{ef}} = 3.7$) of the inlet with contraction ratio $\eta = 3$ does not result in channel blockage when the Reynolds number is high enough ($\mathrm{Re}_{\infty L} = 22 \cdot 10^6$). But when the Reynolds number is significantly lower ($\mathrm{Re}_{\infty L} = 8.5 \cdot 10^6$), the same inlet is blocked at much smaller wedge bluntness $r = 2$ mm ($r/W_t = 0.06$, Fig. 11*a*). At that, the corresponding value of effective contraction ratio for turbulent boundary layer is $\eta_{\mathrm{ef}} = 3.4$.

Figure 11*a* reflects an unexpected fact: at lower Reynolds number $\mathrm{Re}_{\infty L} = 8.5 \cdot 10^6$ and M = 5 and $\eta = 3$, there is a range of related bluntness radii $r/W_t = 0.06$–0.11 ($2 < r < 4$ mm), wherein the inlet can be started and nonstarted as well. This fact will be discussed below.

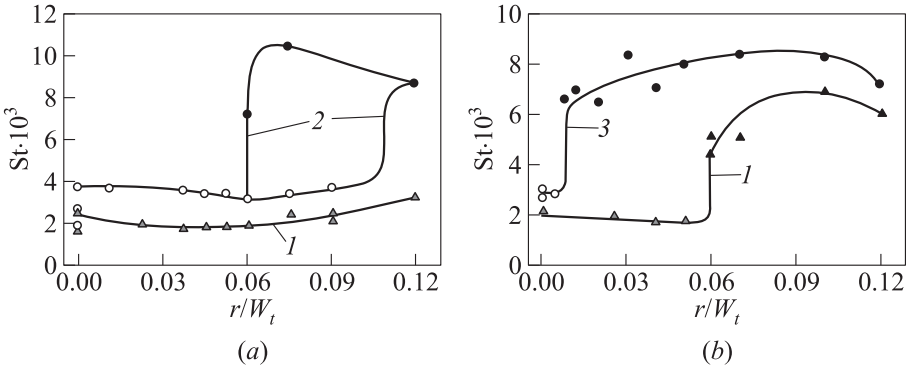

Figure 11 Reynolds number influence on the inlet blockage at M = 5: (*a*) $\eta = 3$; (*b*) $\eta = 4$; *1* — $\mathrm{Re}_{\infty L} = 22 \cdot 10^6$; *2* — $8.5 \cdot 10^6$; and *3* — $\mathrm{Re}_{\infty L} = 13 \cdot 10^6$

At bigger contraction ratio $\eta = 4$, Reynolds number impact on the flow in the inlet gets stronger (Fig. 11*b*): at $\mathrm{Re}_{\infty L} = 22 \cdot 10^6$, the bluntness radius $r = 1.5$ mm ($r/W_t = 0.06$ and $\eta_{ef} = 4.6$) is necessary to block the inlet and at $\mathrm{Re}_{\infty L} = 13 \cdot 10^6$, even very small bluntness radius $r = 0.3$ mm ($r/W_t = 0.012$ and $\eta_{\mathrm{ef}} = 4.3$) is enough for blockage. The reason of so strong Reynolds influence is not defined.

At higher Mach number M = 8 and $\mathrm{Re}_{\infty L} = 5.6 \cdot 10^6$, the inlet with $\eta = 4$ is blocked, when the wedges are even sharp. At that, the corresponding value of effective contraction ratio is $\eta_{\mathrm{ef}} = 4.15$, taking into account characteristics of laminar boundary layer on the wedge surfaces. The inlet with smaller contraction rate $\eta = 3$ can be started with significantly blunted wedges (Fig. 12): at $\mathrm{Re}_{\infty L} = 5.6 \cdot 10^6$, the blockage occurs when the related bluntness radius is $r/W_t = 0.06$ ($r = 2$ mm and $\eta_{\mathrm{ef}} = 3.4$, Fig. 12*a*). Reducing the Reynolds number leads to lower value of critical bluntness radius: at $\mathrm{Re}_{\infty L} = 2.8 \cdot 10^6$, $r/W_t = 0.052$ ($r = 1.75$ mm and $\eta_{\mathrm{ef}} = 3.4$, Fig. 12*b*).

Figure 12 shows that at Mach number M = 8 as well as at M = 5, there is a range of wedge bluntness, wherein the flow regime is ambiguous. At M = 8 and $\mathrm{Re}_{\infty L} = 2.8 \cdot 10^6$, it happens in the ranges $r/W_t \approx 0.05$–0.11, $1.75 \leq r \leq 3$ mm, and $\eta_{\mathrm{ef}} = 3.6$–3.9. This phenomenon is probably was not observed up to now in short duration wind tunnels. Figure 12*b* demonstrates that in the case of regular flow, the Stanton number, measured at the characteristic point ($X = 225$ mm and $Z = 0$), continued to decrease monotonically behind the branching point. It means that the observed phenomenon is not connected with the laminar–turbulent transition. Apparently, the causes of the flow ambiguous lies in uncontrolled differences in forming rate of the flow in the wind tunnel. The differences can, for example, be in the rate of pressure rise or in the degree

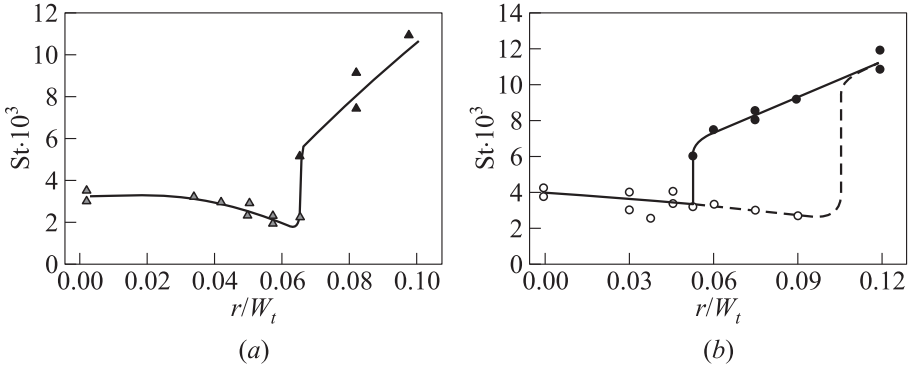

Figure 12 Reynolds number influence on inlet blockage at M = 8 and $\eta = 3$: (*a*) $\mathrm{Re}_{\infty L} = 5.6 \cdot 10^6$; and (*b*) $\mathrm{Re}_{\infty L} = 2.8 \cdot 10^6$

of vacuum before the test run. The other possible reason is the difference in concentration of water vapor in the gas.

8 CONCLUDING REMARKS

Starting of generic inlet with sharp or blunted wedges was investigated experimentally at Mach numbers M = 5 and 8 and Reynolds numbers $\mathrm{Re}_{\infty L}$ from $2.8 \cdot 10^6$ to $22 \cdot 10^6$. The flow structure and heat transfer were studied as well. The inlet was of internal-compression type with flat walls and rectangular cross section.

Increasing the blunting of wedge leading edges results in decreasing of heat transfer until the regular flow structure with internal shocks and local separation zones maintains in the inlet. Exceeding a critical value, depending on the flow characteristics and channel contraction ratio, leads to the inlet blockage and sharp increase of heat flux.

At maximal Reynolds numbers studied, regular flow in the inlet of internal-compression type is possible at contraction ratio up to $\eta = 3$, exceeding significantly the value $\eta \approx 1.6$ for the autostarting inlet. At that, considerable wedge blunting is permissible (up to $r = 2$–4 mm at inlet width 100 mm).

Sensitivity to the wedge blunting enhances with increase of Mach number or channel contraction ratio and with decrease of Reynolds number as well. At high Mach number and low Reynolds number, even small wedge blunting can lead to the inlet blockage.

Ambiguity of flow regime in the inlet is revealed at experiments in the wind tunnel of impulse type: at some flow conditions, there is a range of wedge bluntness wherein subsonic or supersonic flow regime can realize randomly.

At big contraction ratio, the inlet blockage can be accompanied by formation of nonsymmetric separation zone, in which gas flows spirally and backward relative to the undisturbed flow.

The performed experiments confirm applicability of the developed panoramic methods at investigations of the outer and the inner flows, as well.

ACKNOWLEDGMENTS

The research was supported financially by the Russian Foundation for Basic Research in the frame of Projects #11-01-00657 and #14-01-00378.

REFERENCES

1. Kantrowitz, A. 1947. The formation and stability of normal shock waves in channel flows. NACA TN 1225.
2. Abramovich, G. N. 1969. *Applied gas dynamics*. Moscow: Nauka. 824 p.
3. Gurylev, V. G., A. K. Ivanyushkin, and E. V. Piotrovich. 1973. Experimental investigation of Reynolds impact on inlet starting at high supersonic speeds. *Uchenye Zapisky TsAGI* IV(1):33–44. (In Russian.)
4. Starukhin, V. G., and A. F. Chevagin. 1994. Influence of front-end edges bluntness on under-wing intake characteristics. *Uchenye Zapisky TsAGI* V. XXV(1-2):89–100. (In Russian.)
5. VanWie, D. M. 2000. Scramjet inlets. *Scramjet propulsion, progress in aeronautics and astronautics*. Eds. E. T. Curran and S. N. B. Murthy. AIAA. Ch. 7. 189:447–511.
6. Goonko, Y. P., A. F. Latypov, I. I. Mazhul, A. M. Kharitonov, M. I. Yaroslavtsev, and P. Rostand. 2003. Structure of flow over a hypersonic inlet with side compression wedges. *AIAA J.* 41(3):436–447.
7. Falempin, F., and F. Wendling. 2006. Experimental investigation of starting process for a variable geometry air inlet operating from Mach 2 to Mach 8. AIAA Paper No. 2006-4513. 8 p.
8. Neuenhahn, T., and H. Olivier. 2006. Influence of the wall temperature and entropy layer effects on double wedge shock boundary layer interactions. AIAA Paper No. 2006-8136.
9. Häberle, J. and A. Gülhan. 2007. Investigation of the flow field of a 2D scram-jet inlet at Mach 7 with optional boundary layer bleed. AIAA Paper No. 2007-5068. 19 p.
10. Xavier, V., T. Rabi, E. Timofeev, and M. Sannu. 2008. Limiting contractions for starting simple ramp-type scramjet intakes with overboard spillage. *J. Propul. Power* 24(5):1042–1049.

11. Wagner, J. L., K. B. Yuceil,. A. Valdivia, N. T. Clemens, and D. S. Dolling. 2009. Experimental investigation of unstart in an inlet/isolator model in Mach 5 flow. *AIAA J.* 47(6):1528–1542.
12. Mahapatra, D., and G. Jagadeesh. 2009. Studies on unsteady shock interactions near a generic scramjet inlet. *AIAA J.* 47(9):2223–2231.
13. Throckmorton, R., J. A. Schetz, and L. S. Jacobsen. 2010. Experimental and computational investigation of a dynamic starting method for supersonic/hypersonic inlets. AIAA Paper No. 2010-589. 11 p.
14. Tan, H., L. Li, Y. Wen, and Q. Zhang. 2011. Experimental investigation of the unstart process of a generic hypersonic inlet. *AIAA J.* 49(2):279–285.
15. Borovoy, V., I. Egorov, A. Maximenko, V. Mosharov, V. Radchenko, A. Skuratov, and I. Struminskaya. 2013. Three-dimensional shock-wave/boundary-layer interaction at the presence of entropy layer. *Progress in flight physics*. Eds. P. Reijasse, D. D. Knight, M. S. Ivanov, and I. I. Lipatov. EUCASS advances in aerospace book ser. TORUS PRESS – EDP Sciences. 5:327–348.
16. Borovoy, V., I. Egorov, V. Mosharov, V. Radchenko, A. Skuratov, and I. Struminskaya. 2015. Influence of leading edge bluntness on hypersonic flow in a generic internal-compression inlet. *Progress in flight physics*. Eds. D. D. Knight, I. I. Lipatov, and P. Reijasse. EUCASS advances in aerospace book ser. TORUS PRESS – EDP Sciences. 7:419–436.
17. Mosharov, V. E., and V. N. Radchenko. 2007. Izmerenie poley teplovykh potokov v trubakh kratkovremennogo deystviya s pomoshch'yu luministsentnykh preobrazovateley temperatury [Measurement of heat transfer distributions in short duration wind tunnels using luminescent temperature transformers by temperature sensitive paint]. *Uchenye Zapisky TsAGI* 38(1-2):94–101.
18. Mosharov, V.,E., and V. N. Radchenko. 2010. New method of flow visualization on the surface of aerodynamic models. *Sensors Syst.* 5:48–53.
19. Borovoy, V. Ya., A. S. Skuratov, and I. V. Struminskaya. 2008. On the existence of a threshold value of the plate bluntness in the interference of an oblique shock with boundary and entropy layers. *Fluid Dyn.* 43(3):369. doi: 10.1134/S0015462808030058.
20. Zheltovodov, A. A., and D. D. Knight. 2011. Ideal-gas shock wave – turbulent boundary-layer interactions in supersonic flows and their modeling: Three-dimensional interactions. *Shock wave – boundary-layer interactions*. Eds. H. Babinsky and J. K. Harvey. Cambridge University Press. 202–258.